DOI: 10.15480/882.9339

Eighth International Symposium on Marine Propulsors
smp'24, Berlin, Germany, March 2024

Design of a high efficiency podded drive for improved course keeping

Jan Clemens Neitzel-Petersen[1], Reinhard Schulze[2], Simon Froitzheim[2], Uli Bauch[1]

[1]Siemens Energy Global GmbH & Co. KG, Hamburg, Germany
[2]SVA, Potsdam Model Basin, Potsdam, Germany

ABSTRACT

The design of modern podded propulsion solutions is dominated by merging different, partly counteracting requirements at widely spread operating conditions. Whereas high propulsion efficiency is the key factor, large steering forces at small azimuth angles while maintaining reduced azimuth torque are of importance for a safe navigation with reasonable azimuth unit and bearing sizes. The paper introduces the approach to consider the different requirements in the early stage of a pod design of the SISHIP SiPOD 17M by application of numerical methods. Over a period of more than 25 years, the Potsdam model basin has developed optimizing methods for pods using series of model tests and numerical calculations to achieve an integral description of the interactions of propeller and housing. The numerical method is demonstrated by presenting the propeller design tool *VTXopt* with an optimization procedure designed as an inverse method. Enhanced numerical calculations using a RANS solver demonstrate the consequences of different fin and strut configurations on course-keeping and maneuvering. An improved steering capability with an attached fin at the cost of larger azimuth torque at small azimuth angles is observed, whereas the azimuth torque at large angles is reduced. The results are validated by model tests at the SVA Potsdam GmbH (SVA).

Keywords

Pod, course-keeping, design, efficiency

1 INTRODUCTION

Podded propulsion unites the tasks of prime mover and maneuvering device for ships. Whereas conventional prime movers are subjected to oblique inflow of small angles, pods can be turned by up to 180° to the inflow direction. In combination with the rudder-like strut, large loads occur on the structure, drives and bearings. Still, numerical calculations and model tests at oblique inflow contain a significant uncertainty when it comes to scaling to full scale, hence, model tests results in comparison to full-scale simulations are of importance for realistic load estimation during pod azimuthing.

An experimental study carried out by Koesterke & Froitzheim (2022) analyzed different propeller hubs and a pod shape in model scale. The study concludes that different scaling approaches of the loads on contributing parts such as propeller, hub and pod housing are paramount. The procedures and guidelines for model tests and extrapolation to full scale for podded propulsion (ITTC 2017) are analyzed, not recommending simplifications as a replacement of the pod unit assessment. Park et al. (2014) introduced a scaling method for pulling type pods by isolating the hydrodynamic loads by parts and corresponding flow velocity. After comparison of results from model tests and full-scale RANS calculations, scaling factors for an assessment by parts are identified and a scaling procedure is presented.

Wang et al. (2019) assessed an L-type pod in oblique flow numerically and experimentally. Whereas the propulsion characteristics are experimentally evaluated, blade loads, and flow analysis are carried out with numerical methods, excluding a result comparison for the pod in oblique flow. For straight ahead condition, the comparison from experiment to simulation indicates an error of less than 5% for J=0.5-1.0. The trends stated for the propulsion characteristics and their explanation via flow visualization from numerical calculations support the understanding of the occurring phenomena. As shown by Neitzel-Petersen et al. (2021), significant impact on the hydrodynamic loads can also be due to dynamic effects. Increasing the azimuth speed changes the flow situation on the strut delaying separation to larger azimuth angles. An increase in bearing loads of about 20% due to dynamic stall in model tests and RANS calculations is presented. A comparison to quasi-static cases shows an underestimation of loads by 40% at azimuth angles of 30° without consideration of dynamic azimuthing, demonstrating the importance of simulating the pod motion. Chen et al. (2023) carried out RANS calculations of a pod in oblique inflow by varying the advance coefficient and azimuth angle. Comparing the static results and results from dynamic azimuthing at angles of ±50°, a hysteresis effect is observed with bearing load increase at all angles due to dynamic effects.

Attaching fins to the podded propulsor can be used for load balancing and efficiency increase. Yao et al. (2020) evaluated the influence of thrust fins attached to the gondola downstream of the pulling propeller by applying fins of different size and angle of attack. Whereas a significant effect on the gondola resistance was observed, the total thrust and efficiency vary by less than 1% for different fin sizes. No direct comparison to the same operation point without fins is drawn.

2 THEORETICAL APPROACHES

2.1 Propeller design method

The program *VORTEX* calculates the quasi-stationary characteristics of propellers using the lifting surface method (Schulze 1995, 1997 and 2019). In cooperation with postprocessors for a graphical representation *VORTEX* computes the open water characteristic, the pressure distribution, the cavitation behaviour, the forces and moments and the velocity field around the propeller. If an unsteady inflow is defined, *VORTEX* computes in connection with the postprocessor *CAVIPLOT* the quasi-stationary cavitation behaviour in the wake field and in connection with the postprocessor *VTXFORCE* the forces and moments acting on the blades and the propeller (body forces).

The algorithms based on the vortex lattice methods lead to a short computation time and a sufficient accuracy for most applications. In contrast to other vortex lattice algorithms (e.g., Greely & Kerwin 1982) *VORTEX* uses four parameters for a friction correction. All parameters for the friction correction are estimated by an array of measurements with model propellers and have a functional representation with respect to the main propeller characteristics. This ensures a high accuracy, also for propellers with an unconventional geometry. If the parameters for the procedure described in Schulze (2016) are determined with measurements from model propellers, which are scaled to full scale by Reynolds number correction, the *VORTEX* results are valid for full-scale prognosis.

2.2 Numerical flow solver

The numerical calculation of the flow around the pod in full scale are carried out with the RANS solver *Simcenter STAR-CCM+*. A finite volume approach is applied to provide a spatial discretization of the transport equation to approximate the solution of the unsteady, incompressible Reynolds-averaged Navier Stokes equations (RANSE) in the computational domain. The behavior of the fluid is described with the continuity equation,

$$\frac{\partial \rho}{\partial t} + \nabla \cdot (\partial \rho \boldsymbol{u}) = 0, \qquad (1)$$

and the momentum equation,

$$\begin{aligned} &\left(\frac{\partial}{\partial t} + \boldsymbol{u} \cdot \nabla\right)(\rho \boldsymbol{u}) = \\ &-\nabla p + \nabla \cdot (\tau + \tau_T) + f, \end{aligned} \qquad (2)$$

$\forall \boldsymbol{x} \in \Lambda$. The Reynolds-averaged velocity vector is denoted as **u** together with the Reynolds-averaged pressure p. The Reynolds-averaged molecular stress tensor τ and the Reynolds stress tensor τ_T due to the Reynolds averaging are also included. The components of the Reynolds stress tensor due to the Reynolds-averaging are approximated by using the SST k-ω turbulence model by Menter (1992).

2.3 Non-dimensional values

The results of the numerical calculations and model tests are presented as non-dimensional values. The force *F* is divided by the propeller rotation rate *n*, the density of the fluid ρ and the propeller diameter *D*.

$$K_F = \frac{F}{\rho \cdot n^2 \cdot D^4} \qquad (3)$$

An equivalent approach is applied to the values of the torque M.

$$K_M = \frac{M}{\rho \cdot n^2 \cdot D^5} \qquad (4)$$

Result tables contain non-dimensional figures multiplied with an arbitrary number, whereas plots either show relative values or no y-axis scaling, as the podded propulsion unit is a commercial product and key capabilities contain proprietary information.

3 EXPERIMENTAL STUDY

3.1 Case study

The podded propulsor applied in this case study is the SISHIP SiPOD 17M engineered, distributed, and built by the *Siemens Energy Global GmbH & Co. KG*. The pod consists of a strut, a gondola housing with the electric motor and a propeller in pulling arrangement. As visualized in Fig. 1, a fin of variable size can be attached to the lower downstream end of the pod.

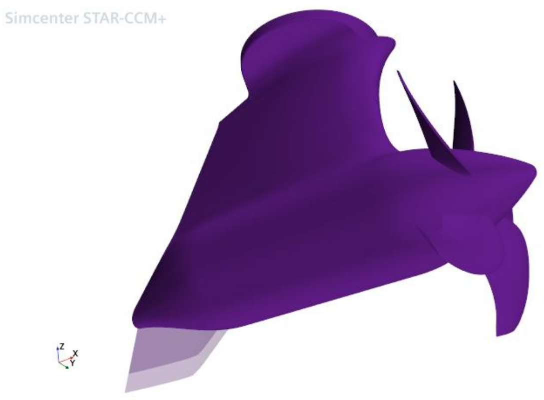

Figure 1: SISHIP SiPOD with attached fin variations

The propeller axis of the case study is not inclined and its vertical distance to the top attachment is 4.3m. The pod has an overall length of 9.6m and a total height of 6.9m. The diameter of the 5-bladed propeller is 5.2m. Two fins can be attached to the downstream end of the gondola housing extending vertically downwards. The small fin ends at 61% of the propeller radius and the large fin covers 77% of the propeller diameter. The fins are modelled using typical profile shapes. For confidentiality reasons, the propeller rotation rate cannot be published, but the propeller advance ratio is around 0.9. All numerical calculations and model tests consider a flow velocity of 22.2kn. The SISHIP SiPOD model is scaled by 1:23.864.

3.2 Experimental setup

To obtain reasonable reference values for the CFD simulations, cavitation tests in homogeneous inflow are carried out at SVA Potsdam. The cavitation tests take place in the large measuring section of the cavitation tunnel K15A of Kempf & Remmers (K&R). The forces of the SISHIP SiPOD 17M with a representative design propeller ($\lambda \approx 24$) are measured with the balance R37 (K&R). The force measuring elements X, Y1 and Y2 are designed for maximum forces of 500 N and the torque for a maximum size of 20 Nm. The z-drive Z600, developed by SVA, is mounted on the R37 balance. The test setup with the scale R37 and the z-drive Z600 (ref. Fig. 2) allows the measurement of the system forces up to 6DoF.

The following test program of the cavitation tests is conducted for three-pod-configurations. The first configuration is not equipped with an additional fin, while the second and third are, as lined out in 4.1.

- Measurement of the pod-characteristic at $\delta_R = 0°$
- Measurement of the pod-characteristic at $\delta_R = \pm 5°$
- Variation of the azimuth angle from $\delta_R = -10°$ to $\delta_R = 10°$ in a test regime of the following order: $\delta_R = 0°$, $\delta_R = 0° \rightarrow -10°$, $\delta_R = 0°$, $\delta_R = 0° \rightarrow 10°$, $\delta_R = 0°$. This procedure proofs a good repeatability. The azimuth angle variation is carried out at OP1 (typical design point).
- Cavitation observation at two operating points

A positive azimuth angle is defined for a clockwise rotation, observed from above.

The observed operating points represent a typical design point of the pod at propulsion and crabbing conditions.

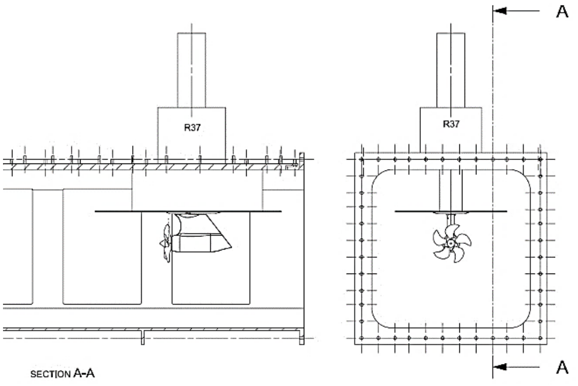

Figure 2: Test arrangement in the cavitation tunnel K15A

Table 1: Operating points

Mode			Design	Crabbing
Cavitation number	σ_n	[–]	2.143	3.902

3.3 Experimental results

3.3.1 Open water

The first objective is to compare the efficiency of the SISHIP SiPOD 17M with different attached fins. Figure 3 shows, that no notable difference between the configurations could be measured with respect to the open water efficiency in the whole range of the advance coefficient (J_k) at $\delta_R = 0°$. Especially the propeller data are almost identical between the different configurations.

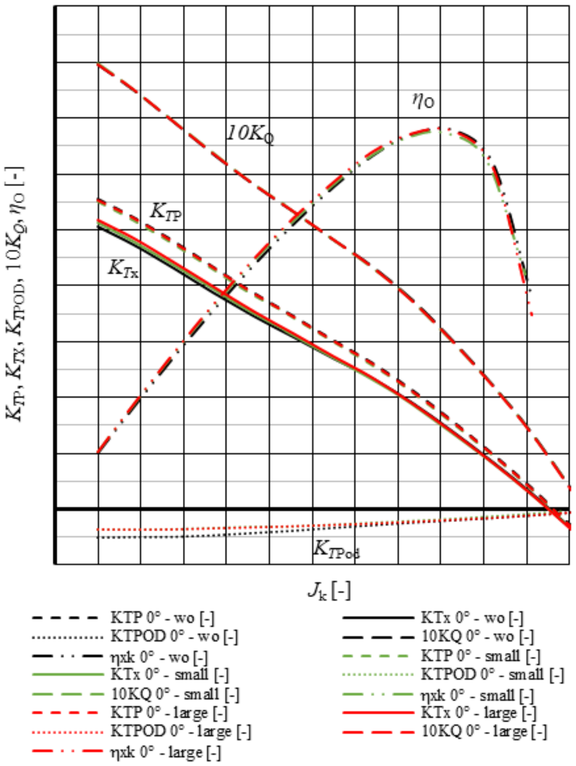

Figure 3: Pod-characteristics, Model scale, 15 rps, black: without fin, green: with small fin, red: with large fin

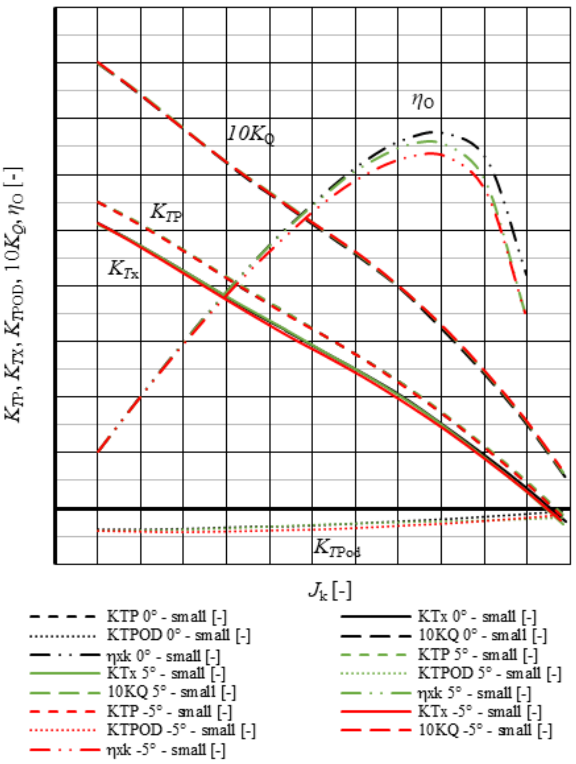

Figure 4: Pod-characteristics small fin, Model scale, 15 rps, black: $\delta_R = 0°$, green: $\delta_R = 5°$, red, $\delta_R = -5°$

When comparing the pod-characteristics for $\delta_R = 0°$ and $\delta_R = \pm 5°$, a difference of open water efficiency at the propulsion point can be found, while the propeller related data ($10K_Q$, K_{TP}) remain the same (ref. Fig. 4). Since bollard pull condition is similar for every angle δ_R, obviously, the coefficients are identical. This measured behaviour can be seen as proof for the validity of the measurements in the cavitation tunnel. The walls of cavitation tunnel have a minor effect, also for small azimuth angles. At higher advance coefficients, the pod resistance increases if a fin is attached. Due to the asymmetry of the propeller slipstream, this effect is not equal for positive and negative azimuth angles.

From the results follows, that it is irrelevant, which fin-configuration is used in respect of open water efficiency at the propulsion point at $\delta_R = 0°$, while a fin might be favourable at bollard pull condition for thrust creation. If the azimuth angle is varied, the efficiency decreases at the propulsion point, if a fin is attached. Since in operation, the azimuth angle usually is varied by $\delta_R = \pm 3°$ to keep the course, the application of a fin in regard to efficiency must be evaluated considering the importance of bollard pull thrust in operation.

3.3.2 Variation of azimuth angle

The model tests with the SISHIP SiPOD cover a range of azimuth angles of $\delta_R = \pm 10°$ at design condition. The forces in x-direction (ref. Fig. 5) are in a range of less than 2% for the pod with the small fin and less than 4% for the pod with the large fin compared to the case without fin.

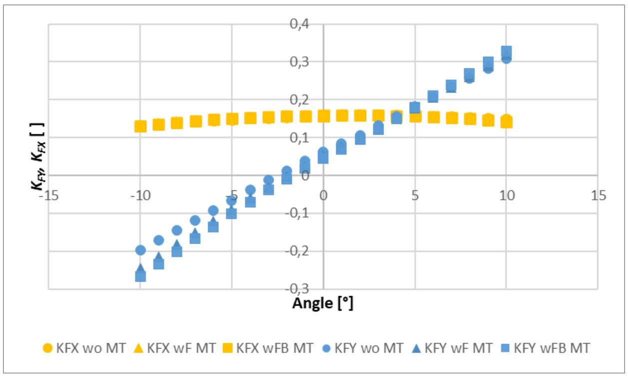

Figure 5: Hydrodynamic forces K_{FX} and K_{FY} (y-axis) from model tests acting on the SISHIP SiPOD with small fin (wF), large fin (wFB) and without fin (wo) at azimuth angles (x-axis) up to $\delta_R = \pm 10°$ from model tests

The curves of the transversal force coefficient K_{FY} for the three cases display similarly small differences for positive azimuth angles above 4°. For negative azimuth angles below -5°, the pod with the small fin creates 24-38% more transversal force than the pod without fin (36-47% for the case with the large fin). Attaching a fin changes the gradient of the K_{FY} curve, shifting the neutral azimuth angle closer to 0° than without a fin. The additional lateral area of the fin and the interaction with the rotating component of the propeller slipstream changes the force balance at the podded propulsor.

As the transversal force created by the attached fin with its location at the downstream end of pod largely influences the azimuth angle, the results of the azimuth torque presented in Fig. 6 are subject to a similar trend as described for Fig. 5. At positive azimuth angles above +4°, the values for the cases with small fin are within a range of -9% to +4% (-12% to +8% for the pod with large fin) compared to the pod without fin. Whereas attaching the small fin reduces the required azimuth torque at angles below -6° to 48-39% of the result without a fin, the large fin demands with 29-13% only a small part of the required azimuth angle without an attached fin. As becomes obvious in Fig. 6, the neutral angle is changing from around -2° to -5° for the case with a large fin. An increased requirement of azimuth torque for the pod equipped with a fin must be stated for -2° to +5°.

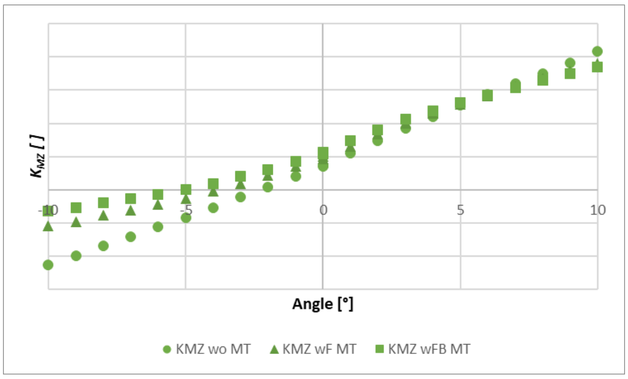

Figure 6: Hydrodynamic azimuth torque K_{MZ} (y-axis) from model tests acting on the SISHIP SiPOD with small fin (wF), large fin (wFB) and without fin (wo) at azimuth angles (x-axis) up to $\delta_R = \pm 10°$ from model tests

3.3.3 Verification study

For verification purposes, the models of the SISHIP SiPOD are tested at an azimuth angle of 0° at the operation point of interest. As the result values are proprietary, the relative bandwidth of 3 measurements divided by the smallest result value is disclosed. The case without fin has a relative bandwidth of 0.8% for the force in x-direction, 1.1% for the force in y-direction and 8.9% for azimuth torque. By attaching the large fin to the pod, the bandwidths are 0.3%, 5.0% and 2.2%. As the values for the azimuth torque and the force in y-direction are small, the results are regarded as sufficient by the authors.

4 Numerical Study

41 Propeller optimization

4.1.1 Design process

The propeller design tool *VTXopt* is built on the numerical kernel of *VORTEX* as an optimization procedure (inverse method) for propellers. The requirements for the propeller design like open water efficiency and the achievable cavitation properties at the design advance coefficient are combined in a weight function, which will be maximised / minimised by numerical optimization techniques. Based on the calculation methods in *VORTEX*, an inverse method for determining an optimal propeller geometry was implemented using an optimization tool.

The definition of an evaluation criterion f(G): f(G) = f(G, J^*, $\eta_O(J^*)$, $\sigma_n(J^*)$, $k_Q(J^*)$) is realized in such a way that f(G) is minimal, if $\eta_O(J^*)$ is maximal, $\sigma_n(J^*)$ minimal and $k_Q(J^*) = k_Q^*$, with predefined J^* and k_Q. J^* represents the design advance coefficient of the respective propeller.

$\eta_O(J^*)$, $\sigma_n(J^*)$, $k_Q(J^*)$ can be calculated with an “arbitrary” propeller calculation code. The propeller geometry is defined by a finite set of real numbers derived from a polynomial representation of the radial distributions of pitch, camber, skew and rake.

There are various algorithms available for solving the minimization problem such as Newton-like algorithms (Davidson-Fletcher-Powell) as well as direct-search-algorithms (Gablonski-algorithm).

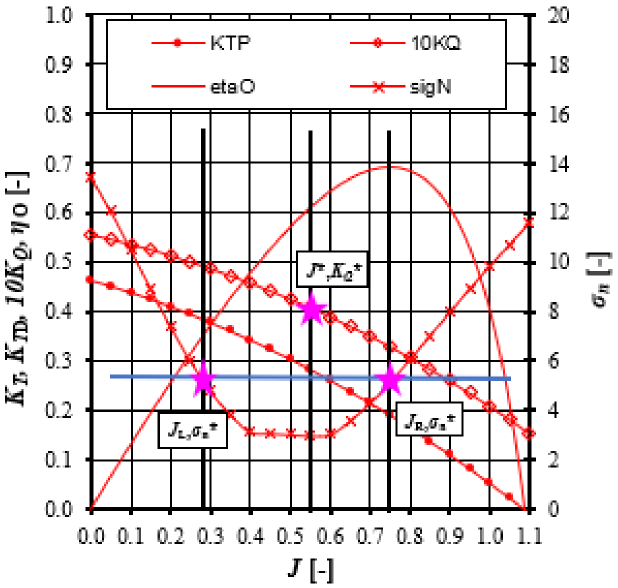

Figure 7: Multi-objective optimization of the open water characteristics of a propeller

These methods are integrated in the SVA propeller code *VTXopt* with the main tools of the program package *VORTEX*. *VTXopt* is defined in such a way, that a multi-objective optimization is possible. This is presented in Fig. 7: For different advance coefficients different restrictions can be defined.

4.1.2 Case study & results

Using the example of a ship with a top speed of 22.2 kn, a propeller pod application with the SISHIP SiPOD 17M drive must be designed due to power and torque requirements.

The shape of the pod gondola has an essential influence on the hydrodynamic parameters of a podded propulsion device. This has been studied extensively by Heinke (2001 and 2004) and Schulze (1999, 2011) and leads to an algorithm to calculate the interaction of pod and propeller. Initially, the open water curve of the pod-propeller system can be calculated from the “pure” open water characteristic of the propeller.

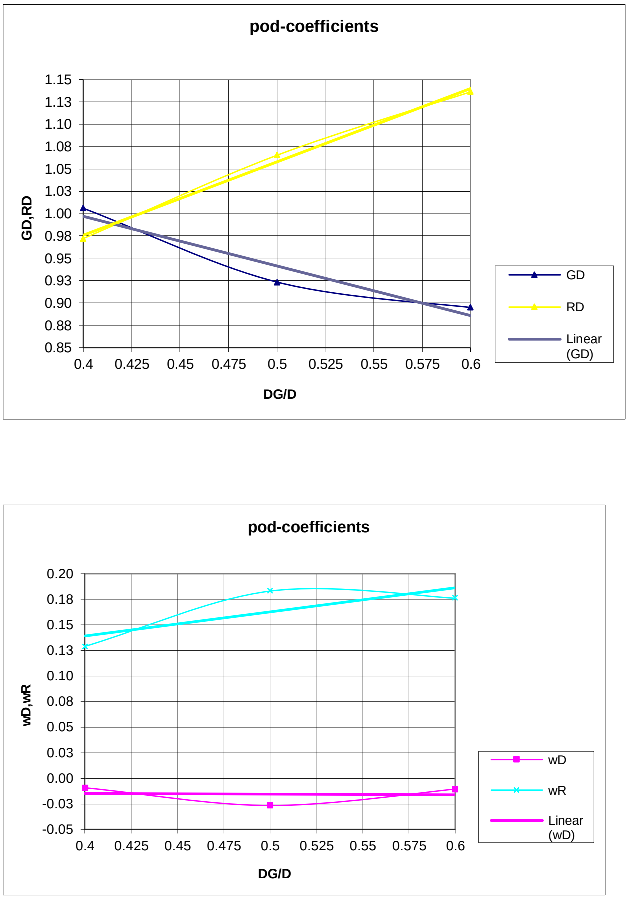

Figure 8: Gondola coefficients plotted over the gondola diameter (D_G) divided by propeller diameter (D)

In dependency of gondola length and diameter, a set of four parameters (G_D, w_D, R_D, w_R) to describe the following formulas are introduced.

$$k_{T(gondola)}(J) = G_D \cdot k_{T(open\ water)} \cdot (J \cdot (1 - w_D)) \tag{5}$$

$$k_{Q(gondola)}(J) = R_D \cdot G_D \cdot k_{Q(open\ water)} \cdot (J \cdot (1 - w_D) \cdot (1 - w_R)) \tag{6}$$

Based on experiments with systematically modified gondola diameters and lengths, the parameters (G_D, w_D, R_D, w_R) are derived in such a way that the minimum of the following functional f was determined for this set of measurements:

$$f(G_D, w_D, R_D, w_R) = \int \Big(k_{T(gondola)}(J) - G_D \cdot k_{T(open\ water)} \cdot \big(J \cdot (1 - w_D)\big)^2 + k_{Q(gondola)}(J) - R_D \cdot G_D \cdot k_{Q(open\ water)} \cdot \big(J \cdot (1 - w_D) \cdot (1 - w_R)\big)^2\Big)\, dJ, \tag{7}$$

where the integral was to be determined over the interval (J_{min}, J_{max}).

The minimum problem has a unique solution. The dependency of the gondola geometry on these parameters is summarised in Figures 8 and 9 (Schulze 2011). This set of formulas is integrated in the program *PodPar*.

The four parameters are derived for our design task from the curves in Figures 8 and 9. Then, the open water characteristic of the designed propeller is calculated by *VORTEX*, and by using *PodPar* the interaction of propeller and pod is considered. These results are compared in Figure 10 correlating with the measurements of different model basins.

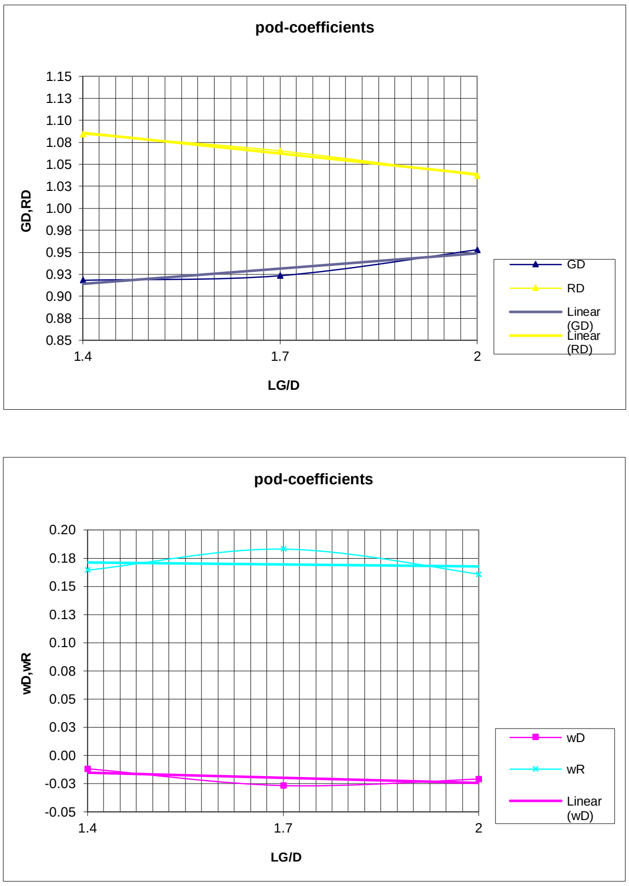

Figure 9: Gondola coefficients plotted over the gondola length (DG) divided by propeller diameter (D)

At last the nominal wake field of the ship is required to calculate the cavitation properties of the propeller. The difficulty of a pull propeller arrangement is the fact, that a displacement body (the pod housing) is located downstream of the propeller, which cannot be neglected. It has been shown in the past that it is possible to calculate the ship's wake in the propeller plane by using CFD methods and, separately, to determine the stagnation effects on the pod housing using CFD methods (or wake measurements). Both effects can be superimposed.

The resulting inflow (combined nominal wake field w_{COM}) to the propeller is calculated by $w_{COM} = \alpha * w_S + (1-\alpha)\ w_{Pod}$ with $\alpha \sim 0.7$ (with w_S as ship's wake and w_{Pod} as stagnation effect of the pod, ref. Fig. 11).

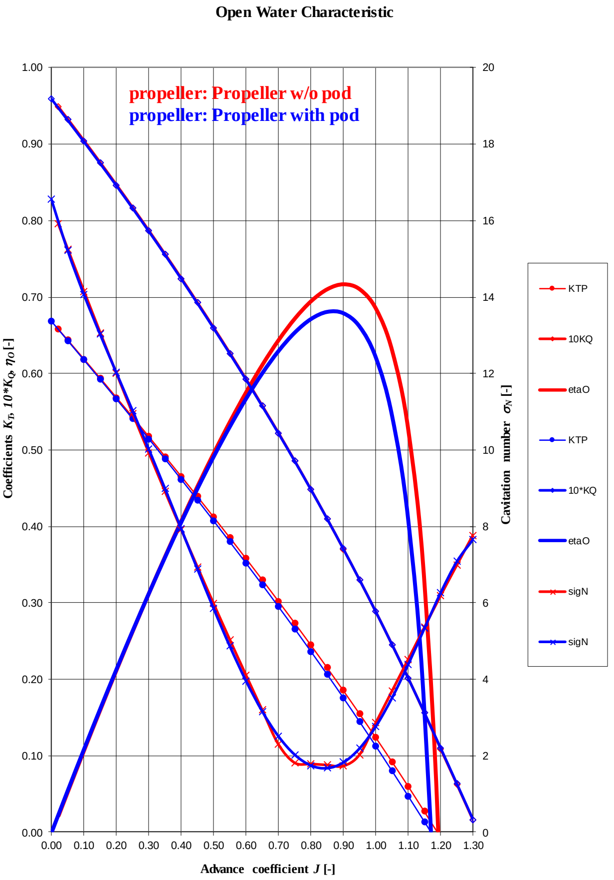

Figure 10: Comparison of the pure open water characteristic (red) and the open water characteristic with interaction with pod housing (blue) (calculated with VORTEX)

The inception of sheet cavitation can be calculated using the potential flow code VORTEX. If the value of the pressure calculated on a patch is below vapor pressure, the patch is treated as cavitating. It can be interpreted as a conservative estimation of the extension of sheet cavitation. The inception of tip vortex cavitation requires an additional model. The model from the code UNCA99 (Szantyr 1993) was applied, where an empirical correlation of tip surface pressure to tip vortex cavitation is included. The result of the cavitation properties in the combined wake for the speed of 22.2 kn is presented in Fig. 12. The tip design as applied to this propeller with a sophisticated pitch, camber and thickness distribution ensures in general a significantly reduced risk of tip vortex cavitation and a high efficiency in common operation modes.

The program UNCA99 calculates the corresponding pressure pulses in the wake. The calculated pressure pulses (1^{st} order) at a tip clearance of 0.3D with a maximum of 0.84 kPa in the position above the propeller are significantly lower than 1 kPa.

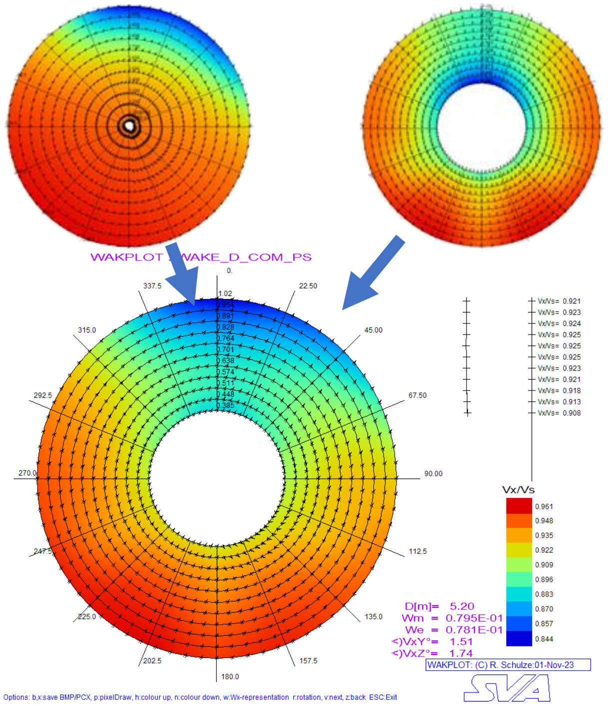

Figure 11: Combined wake field from ship (upper left), gondola (upper right) to total wake (lower center)

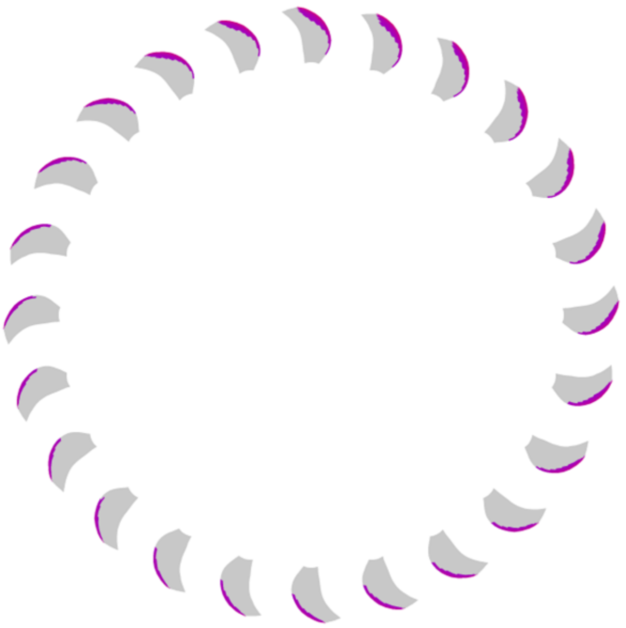

Figure 12: Blade cavitation evaluation demonstrating a small risk of stable sheet cavitation on suction side

The propeller design process as presented in this section is applied to determine an optimized podded propulsion solution by numerical means, considering the operation points, ship influence and pod interaction. The results of the open water characteristic and propulsion prognosis for this case study around the design point are within a range of ±1% of the model test values. The pressure pulses are overestimated by about 15% at location with maximum values. The general trend in comparison to full-scale prognosis from model testing (not presented here) supports the expectation of a conservative, yet precise prediction method.

4.2 Course-keeping and steering

4.2.1 Numerical setup

The pod is in an outer domain of rectangular shape. The inlet is located 4 pod lengths upstream of the azimuth axis and the pressure outlet is placed at 8 pod lengths downstream. The distance to the sides of the domain is about 4 pod lengths. The distance from the propeller axis to the bottom of the domain is about two propeller diameters. Top, bottom and side surfaces are characterized with a no-slip boundary condition. The semi-sphere surrounding the podded propulsor (green, ref. Fig. 13) has a diameter of about 2 pod lengths, containing the pod and propeller cylinder (light blue) with a diameter of 1.2 times the propeller diameter. The semi-sphere can be rotated around the pod's azimuth axis and the propeller cylinder rotates around the propeller axis to depict all relevant motions.

Figure 13: SISHIP SiPOD with propeller domain and pod domain

The coordinate system is placed at the intersection of the azimuth axis with the top surface of the outer domain. The x-axis is oriented against the inflow direction and the z-axis points orthogonal to the top surface upwards away from the pod.

The unstructured mesh consists of three separate domains connected with boundary interfaces. The outer domain outside of the pod domain contains a coarse meshing approach to model the outer flow. Close to the pod domain, several refinement regions increase the mesh density in sensitive areas. Inside the pod domain, a fine mesh is applied to cover the flow details around the housing. Density regions increase the mesh count around the strut and along the propeller slip stream. The propeller domain contains a fine mesh for the propeller. Similar surface meshing conditions are applied on the connecting interface sides.

The near-wall flow on the surfaces with a no-slip boundary condition is modelled using prismatic cells. The height of the prismatic cells corresponds to the boundary layer of a turbulent flow approximated following Schlichting and Gersten's (2000) formula:

$$\delta = 0.37 \cdot L \cdot \left(\frac{U_\infty \cdot L}{\nu}\right)^{-1/5}, \qquad (8)$$

with L as the run length, U_∞ as the flow speed and ν as the kinematic viscosity of water.

The near-wall layer height of the prismatic cells corresponds to the desired wall-y^+-value, which for full scale is above 100.

All numerical calculations are carried out as time-dependent simulations with a time step size corresponding to 5° of propeller rotation. The calculation time is set until reaching a time-averaged value of constant size over several blade passage periods. The time-averaged values of the last 5 blade passage periods are regarded as the result of quasi-stationary calculations.

4.2.2 Results

For the assessment of the forces and azimuth torque acting on the SISHIP SiPOD propulsor, CFD calculations in full scale have been carried out covering the angles from 0° to ±15°. For each angle of attack, the pod has been turned around the azimuth axis, resulting in an oblique inflow on the propeller axis for angles above 0°. The results for the forces in stationary x- and y-direction, corresponding to the ship heading direction, are presented in Fig. 14. For each coordinate direction, results for the pod without (wo), with a small (wF) and with a large fin (wFB) can be found. The results in x-direction indicate a neglectable influence of the size of the fin. For azimuth angles up to ±5°, the results differ by less than ±1% with a decrease to -3% at ±10°. The reduction of thrust in x-direction at ±15° with the smaller fin is about 8% and about 20% with the large fin.

The steering force in y-direction must be interpreted separately for positive and negative azimuth angles due to significant influences of the rotating component of the propeller slipstream. At 0°, the small fin reduces the transversal force compared to the case without fin by 34%. Similar, the force in y-direction of the pod with a large fin is at 45% of that on the pod without fin. Whereas the y-force at an azimuth angle of +1° is around 85% with the small fin and at 78% with the large fin, respectively, compared to the case without fin, the difference vanishes at an angle of +5°. At large angles between +10° and +15°, the steering force of the case with the small fin is 7% larger than that of the case without fin. A similar comparison for the case with the large fin shows an increase of 11%.

At negative azimuth angles, the fins influence the neutral azimuth angle (no steering force) in between 0° and -2°. For angles smaller than -5°, the force in y-direction of the case with the small fin is about 30% larger (about 40% for large fin) than the case without fins.

The azimuth torque is shown in Fig. 15. At 0°, the azimuth torque to keep the pod in position is 74% larger for the case with a small fin and 112% larger for the case with a large fin, respectively, compared to the case without fin. At positive azimuth angles up to 5°, the case without fin requires less azimuth moment for steering. At larger azimuth angles, the cases with fins reduce the torque demand significantly with 24% and 33% less.

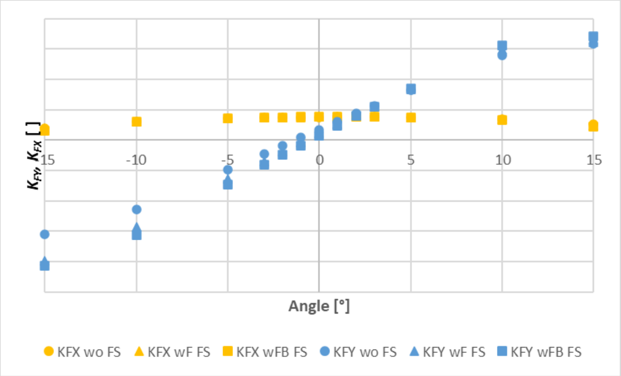

Figure 14: Hydrodynamic forces K_{FX} and K_{FY} (y-axis) acting on the SISHIP SiPOD at azimuth angles (x-axis) up to ±15° from RANS full-scale calculations

At negative azimuth angles, a similar behavior regarding the neutral angle to the steering force is observed. At azimuth angles below -10°, the required torque is reduced to 50% with the small fin and 30% with the large fin compared to the case without fin.

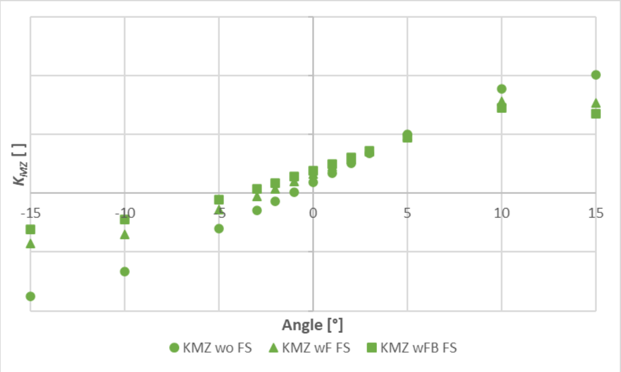

Figure 15: Hydrodynamic azimuth torque K_{MZ} (y-axis) acting on the SISHIP SiPOD over azimuth angles (x-axis) up to ±15° from RANS full-scale calculations

As ships with podded propulsion are usually equipped with two propulsion units with opposite directions of propeller rotation, the steering forces must be combined contrary and the absolute value of the azimuth torque as the required steering power can be added up. The total steering force for the two-pod setup is point symmetric to the origin of the coordinate system and the total azimuth torque is symmetric to the y-axis in Fig. 16. Comparisons indicate a significant increase of azimuth torque with a comparably smaller increase of the steering force at angles below 2°, meaning the applied fins in this case study induce a higher torque during course-keeping. As course-keeping is the main operational condition for conventional ships, applying a fin increases the size of the azimuth unit, as the azimuth drive and the gears must withstand the larger main lifecycle loads acting on a pod with a fin.

At azimuth angles above 2°, less azimuth torque is required to turn and locate the SISHIP SiPOD with fins in comparison to the case without fin. Hence, the required maximum azimuth torque of the azimuth unit is reduced by applying a fin.

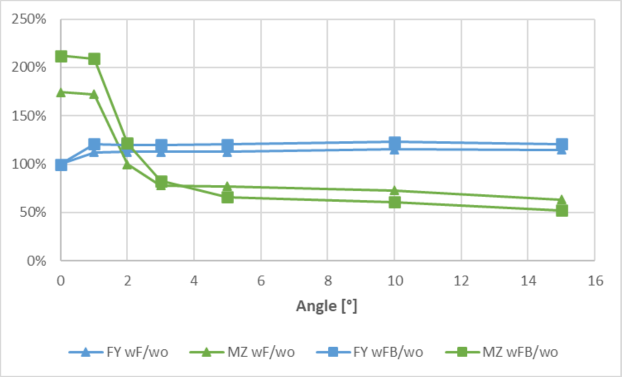

Figure 16: Relative required azimuth torque *MZ* and steering force *FY* (y-axis) for cases with small (wF) and large fin (wFB) compared to the case without fin (wo) for a two-pod setup at azimuth angles (x-axis) up to ±15°

4.2.3. Verification & Validation with model test results

For verification purpose, a mesh convergence study is carried out by scaling the global base mesh size with the factor $r_k = \sqrt{2}$, whereas the near-wall prismatic cell layers are not changed. A study on the influence of the time-step size contains a factor of $r_k = 2$. The procedure is according to the suggested process by Stern et al. (2006), where the changes from the medium to the fine discretization are denoted with $\varepsilon_{k_{21}} = \hat{S}_{k_2} - \hat{S}_{k_1}$ and from the coarse to the medium discretization with $\varepsilon_{k_{32}} = \hat{S}_{k_3} - \hat{S}_{k_2}$. The convergence ratio is defined as:

$$R_k = \varepsilon_{k_{32}} / \varepsilon_{k_{21}}. \qquad (9)$$

Four conditions of convergence behavior are indicated:

i. Monotonic convergence: $0 < R_k < 1$,
ii. Oscillatory convergence: $R_k < 0; |R_k| < 1$,
iii. Monotonic divergence: $R_k > 1$,
iv. Oscillatory divergence: $R_k < 0; |R_k| > 1$.

Divergence conditions iii and iv describe a scenario, where the uncertainties cannot be estimated. In case of an oscillatory convergence, the uncertainty must be estimated by the bandwidth of the oscillatory result limits:

$$U_k = \frac{1}{2}(S_U - S_L). \qquad (10)$$

In case of monotonic convergence (i), the Richardson extrapolation is applied to estimate the error $\delta^*_{RE_{k1}}$ and the order of accuracy p_k:

$$\delta^*_{RE_{k1}} = \frac{\varepsilon_{k_{21}}}{r_k^{p_k} - 1}, \qquad (11)$$

$$p_k = \frac{\ln\left(\varepsilon_{k_{32}} / \varepsilon_{k_{21}}\right)}{\ln(r_k)}. \qquad (12)$$

With the values from eq. 11 and eq. 12, the uncertainty can be calculated as follows:

$$C_k = \frac{r_k^{p_k} - 1}{r_k^{p_{k_{est}}} - 1}, \qquad (13)$$

where $p_{k_{est}}$ is the theoretical accuracy of the numerical method.

For an azimuth angle of 15°, the convergence of the forces with the small fin in x- and y-direction is monotonic. Whereas an uncertainty of 9.60 % of the result for the fine mesh in x-direction is regarded as high, the corresponding value is small, because the large azimuth angle reduces the thrust. For the dominating force in y-direction, the uncertainty is 0.03 % of the result for the fine mesh. The mesh uncertainty regarding the azimuth torque is for oscillating convergence condition at 0.49 % of the result for the fine mesh.

Table 2: Mesh convergence study at 15° for the case with small fin (Result columns multiplied with random value)

	K_{FX}	K_{FY}	K_{MZ}
Coarse	1.088E-2	3.382E-1	3.225E-2
Medium	1.099E-2	3.362E-1	3.194E-2
Fine	1.109E-2	3.353E-1	3.207E-2
R_k	0.9196	0.4964	-0.4298
Condition	i	i	ii
C_k	0.0874	1.015	X
UK % Fine	9.60	0.03	0.49

The results of the convergence study for the time step size show oscillating convergence for the force in x-direction and monotonic convergence for the force in y-direction. With uncertainties of 2.35 % and 0.76 %, respectively, of the result for the case with 2.5° of propeller rotation per time step, reliable results are expected. The monotonic convergence for the azimuth torque results in 6.26 % of the case with the smallest time step.

Table 3: Time step study at 15° for the case with small fin (Result columns multiplied with random value)

	K_{FX}	K_{FY}	K_{MZ}
10.0°/step	1.058E-2	3.425E-1	4.216E-2
5.0°/step	1.109E-2	3.353E-1	3.207E-2
2.5°/step	1.100E-2	3.316E-1	2.778E-2
R_k	-0.1820	0.5054	0.4249
Condition	ii	i	i
C_k	X	0.3262	0.4510
UK % Fine	2.35	0.76	6.26

Comparisons of the results from full-scale CFD calculations and model tests can be seen in Fig. 17 and 18. The comparisons for the cases without fin and with the large fin indicate a good agreement of the trends of the curves for steering force and azimuth torque. A small horizontal shift of the steering forces is observed, resulting in a difference between 3% to 13% for the case without fin and 4% to 14% for the case with large fin in relation to the result value at +10° from the model test.

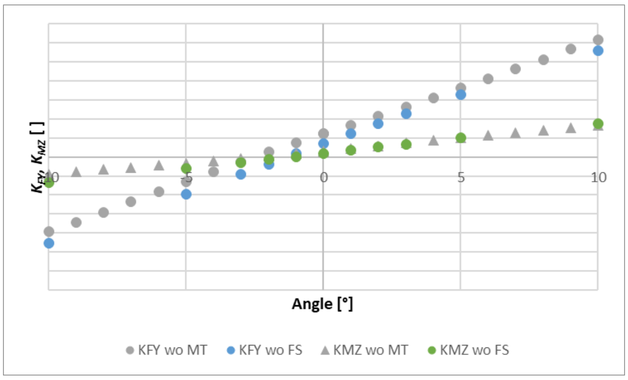

Figure 17: Results from full-scale CFD calculations and model tests for steering force K_{FY} and azimuth torque K_{MZ} (y-axis) at azimuth angles (x-axis) up to ±10° for the case without fin

The difference of the calculated and measured values for the azimuth torque is between 3% and 18% for the case without fin and 3% to 13% for the case with the large fin in relation to the result value at +10° from the model test.

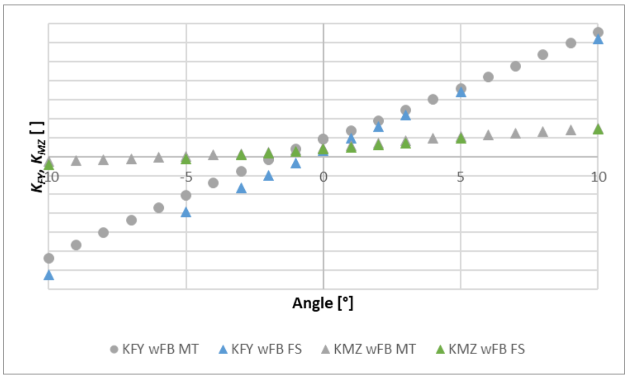

Figure 18: Results from full-scale CFD calculations and model tests for steering force K_{FY} and azimuth torque K_{MZ} (y-axis) at azimuth angles (x-axis) up to ±10° for the case with large fin

The shift of the presented curves of transversal force and azimuth torque regarding the neutral angle can be interpreted as a small shift in angular position of less than 1°, which is inside an error band of the orientation of the pod to the flow in model tests, resulting in a smaller deviation than described above.

4.3 Maneuvering

4.3.1 Numerical setup

Quasi-static calculations at different azimuth angles result in an increase of azimuth moment for cases with attached fins at small azimuth angles. During maneuvering and course keeping, azimuthing is a dynamic process with the pod being steered around 0° or to larger angles. For design ship speed, the pod azimuth angle is often limited to ±35° with an azimuth rotation rate of 3°/s. In order to record the extreme values of the occurring steering forces and moments during maneuvering, the pod is simulated rotating to 35° from straight ahead, over to -35° and back to 0° as shown in Fig. 19.

The maneuver covering the permissible azimuth angles during so-called operation setting “Sea Mode” is carried out with the cases without and with fins.

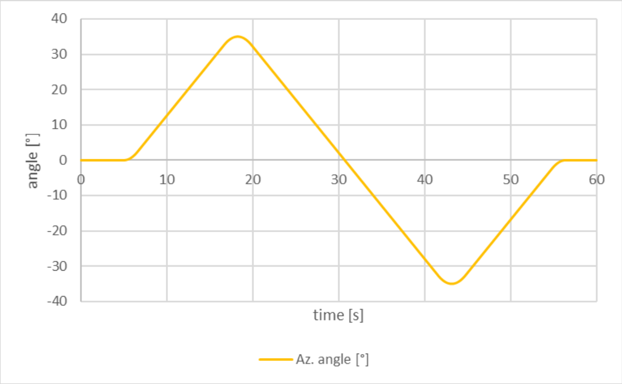

Figure 19: Azimuth angle over time during maneuvering simulation

4.3.2 Results

The trends of the curves for the force in x-direction (thrust direction) indicate a hysteresis (ref. Fig. 20). With increasing absolute value of the azimuth angle, the pod generates less thrust and intersects with the x-axis at smaller absolute angles. Returning to 0°, the pod generates more thrust at similar azimuth angles. With a small fin attached to the pod, the thrust values are similar to the case without a fin. At ±20°, the attached small fin reduces the thrust of about 50% of the case without fins. The case with the large fin shows a small decrease of a few percent compared to the case with fins. For maneuvering with large steering angles, the pod delivers significantly less forward thrust.

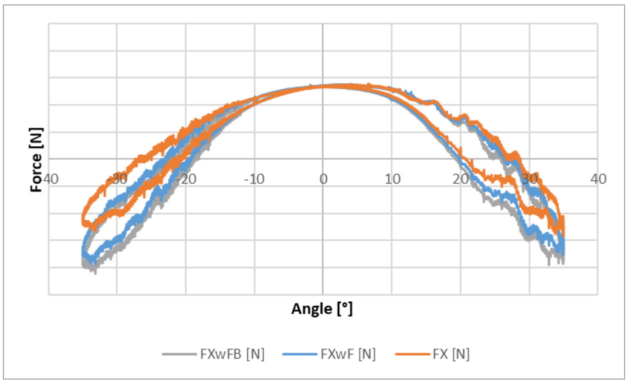

Figure 20: Results from full-scale CFD calculations for the force in x-direction (ship longitudinal direction) at dynamic steering between ±35°

The steering force in y-direction for the three cases is plotted in Fig. 21. A hysteresis with a larger absolut force for increasing absolut azimuth angles is observed, where the pod setups with small or large fin create about 20-30% larger steering forces than the case without attached fin.

During return to an angle of 0°, the difference between the cases is similar to that at increasing absolute angles.

The results in Fig. 22 show a significant influence of the attached fins on the required azimuth torque for steering the pod to the desired angle. For negative azimuth angles, the required torque with fin is about 20-30% of the required torque without fin at angles below -20° and around 50% between 0° and -20°. At positive azimuth angles, the average reduction of required torque is about 30% at 20° and 50% at 30°.

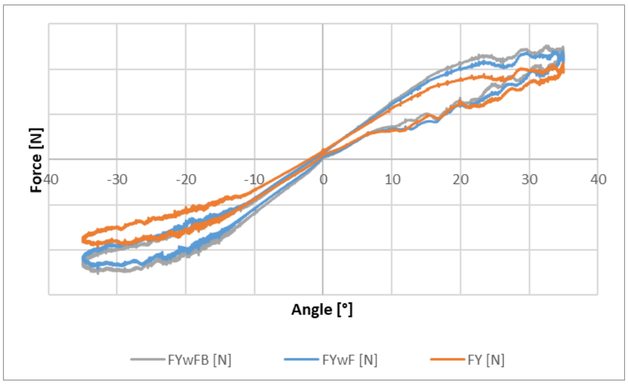

Figure 21: Results from full-scale CFD calculations for the force in y-direction (ship transversal direction) at dynamic steering between ±35°

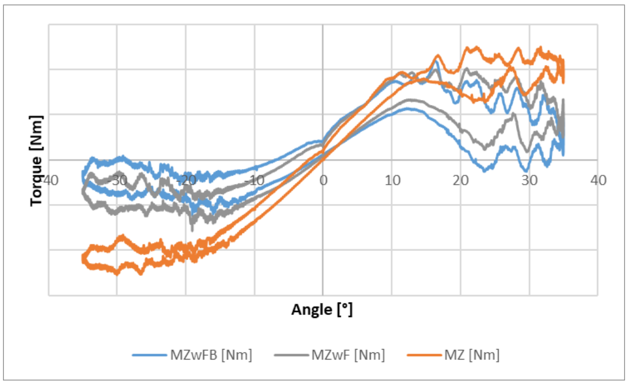

Figure 22: Results from full-scale CFD calculations for the azimuth torque at dynamic steering between ±35°

Additionally, the curves in Fig. 22 cannot be treated as almost point symmetric due to the tangential velocity components of the propeller slipstream acting on the strut, which is more emphasized here than in Fig. 20 and 21.

To demonstrate the importance of the consideration of dynamic steering processes to assess the loads acting on the pod, the results from quasi-static calculations from *5.2.2* and dynamic steering simulation from Fig. 21 are combined in Fig. 23. The results from quasi-static angular positions for the case without fin and with the large fin cover the average value of the occurring forces during dynamic maneuvering, whereas a significant difference for ±15° from maximum dynamic to static force is observed.

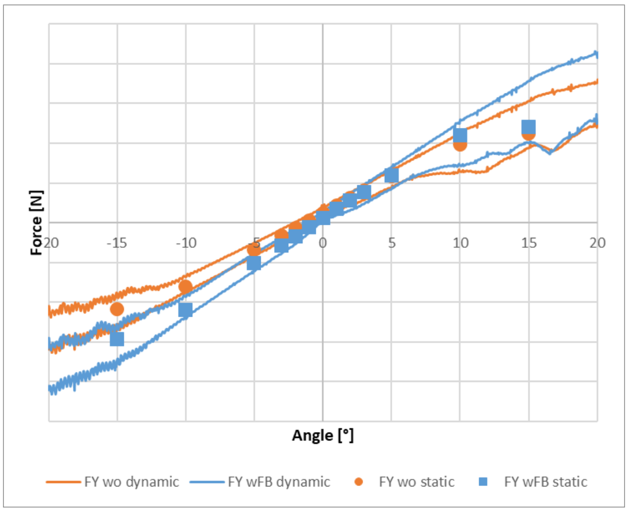

Figure 23: Results from full-scale CFD calculations for the force in y-direction (ship transversal direction) for dynamic steering and static angles between ±20°

5 CONCLUSIONS & OUTLOOK

The paper summarizes the considerations regarding hydrodynamics applied for designing a SISHIP SiPOD. By subdivision in propeller design and pod shape analysis, the presented process mirrors the commercially applied procedure.

The design of the propeller with support of the potential flow solver *VORTEX* considers the influence of the ship and the pod on the wake field. The propeller is optimized by integrating the flow solver in a multi-objective optimization to include requirements such as different operation points or cavitation limits. The process as described carries out a detailed analysis of the influence of strut and gondola shape on the propulsor, leading to an exact prognosis of open water and propulsion efficiency, cavitation occurrence and pressure pulses.

The podded device is analyzed in full scale using the RANS code *Simcenter Star-CCM+* with a focus on the application of fins for maneuvering and course-keeping. The fin location on the downstream end of the pulling-type pod increases the steering forces at azimuth angles above ±5° by about 10%, coming along with a reduction of azimuth torque by up to 75%. At an azimuth angle of 0°, applying a fin reduces the transversal force per pod by 34% and increases the azimuth torque by 112% for the largest fin in scope. For a two-pod solution of a conventional ship, the increased steering force during course-keeping comes at the cost of a double azimuth torque demand, directly increasing the azimuth motors and gears. Hence, the application of fins must be evaluated regarding operation profile.

Model tests with the SISHIP SiPOD show no differences in open water efficiency due to a fin at design point. Close to bollard pull, the fins increase the thrust by recovering rotational energy from the propeller slipstream. By comparing measured values for azimuth angle variation with the full-scale results from numerical assessment, a small shift of the trends along the axis containing the azimuth angle is observed, which leads to deviations of about 5-10%. A good agreement can be obtained, validating the results from numerical calculations.

As the case study in this paper does not consider a variation of the position of the fin, further research shall focus on the influence of varying fin locations on the steering force and azimuth torque. By changing the shape of the pod strut, another influencing parameter can be analyzed to modify the hydrodynamic behavior.

REFERENCES

Breslin, J. P., Andersen, P. (1994). 'Hydrodynamics of ship propellers'. Cambridge Ocean Technology Series 3, Cambridge University Press, 1994

Chen, W., Ma, J., Hu, J. & Zhang, l. (2023). 'Numerical Simulation of Hydrodynamic Performance of Podded Propulsion under Maneuvering Condition'. Journal of Marine Science and Engineering 11 (2023): pp. 874

Greely, D. S. & Kerwin, J. E. (1982). 'Numerical Methods for Propeller Design and Analysis in Steady Flow'. SNAME, Vol. 90, 1982, pp. 415-453

Heinke, H.-J. (2001). 'Alternative Propulsion Concepts for Fast Navy Ships; Part II: Podded drives for navy ships'. STG-Sprechtag, Potsdam, Germany.

Heinke, H.-J. (2004). 'Investigations about the forces and moments at podded drives'. First International Conference on Technological Advances in Podded Propulsion, Newcastle, United Kingdom.

ITTC (2017). 'Podded Propulsion Tests and Extrapolation'. ITTC – Recommended Procedures and Guidelines, Zürich, Switzerland.

Koesterke, M. & Froitzheim, S. (2022). 'Isolated Consideration of Influence Factors in Open Water Tests of Podded Propulsion Systems'. Proceedings of 7th International Symposium of Marine Propulsion, Wuxi, China.

Menter, F. (1992). 'Improved two-equation k-omega turbulence models for aerodynamic flows'. NASA Technical Memorandum, Moffett Field, CA.

Neitzel-Petersen, J.C., Stutz, S.J. & Abdel-Maksoud, M. (2021). 'Steady and Unsteady Hydrodynamic Loads on the Azimuth Bearing of a POD during a Crash-Stop Maneuver'. Journal of Ship Research 65 (2021): p. 25-40

Park, H.-G., Choi, J.-K. & Kim, H.-T. (2014). 'An estimation method of full scale performance for pulling type podded propellers'. International Journal of Naval Architecture and Ocean Engineering, Vol. 6, Issue 4, 2014, pp. 965-980.

Schlichting, H. & Gersten, K. (2000). Boundary-Layer Theory, 8th Edition, Springer-Verlag, Berlin, Germany.

Schulze, R. (1997). 'Globale Optimierung von Propellern'. Jahrbuch der Schiffbautechnischen Gesellschaft, Vol. 91, 1997, p. 97-104, Springer-Verlag Berlin Heidelberg New York, 1997.

Schulze, R. (1995). 'Nachrechen- und Entwurfsverfahren für den Propellerentwurf'. SVA-Forum, SVA Potsdam GmbH

Schulze, R. & Weber, A. (2011). 'Application of the new FORTJES® Z-drive from REINTJES on planing vessels'. 11th International Conference on Fast Sea Transportation FAST 2011, Honolulu, Hawaii, September 2011.

Schulze, R. (2016). 'A new friction correction method for the open water characteristics of propellers'. Jahrbuch der Schiffbautechnischen Gesellschaft, Vol. 110, 2016, p. 42 – 48, Schifffahrts-Verlag „Hansa“ GmbH & Co. KG, Hamburg, 2016.

Schulze, R. (2019). 'Design strategies for noise optimized propellers for multiple screw ships'. Jahrbuch der Schiffbautechnischen Gesellschaft, Vol. 113, 2019, p. 325 – 335, Schifffahrts-Verlag „Hansa“ GmbH & Co. KG, Hamburg, 2019.

Stern, F., Wilson, R. & Shao, J. (2006). 'Quantitative V&V of CFD simulations and certification of CFD codes'. International Journal for Numerical Methods in Fluids, Volume 50, No. 11, April 2006, pp. 1335-1355.

Szantyr, J. (1993). 'UNCA93 the lifting surface program for hydrodynamic analysis of marine propellers'. Report No. RH-93/R-064, Centrum Techniki Okretowej, Gdansk, 1993.

Wang, W., Zhao, D., Guo, C. & Pang, Y. (2019). 'Analysis of Hydrodynamic Performance of L-Type Podded Propulsion with Oblique Flow Angle'. Journal of Marine Science and Engineering 7 (2019): p. 51

Yao, Z., Liu, W., Xu, L. & Ling, H. (2020). 'Influence of thrust fins on hydrodynamic performance of pod propeller'. IOP Conference Series: Earth and Environmental Science, vol. 461, 1.